An application of the spheroidal-coordinate-based transition matrix: The acoustic scattering from high aspect ratio solids

Roger H. Hackman and Douglas G. Todoroff
Naval Coastal Systems Center, Panama City, Florida 32407

(Received 29 March 1984; accepted for publication 22 April 1984)

In a previous paper [Roger H. Hackman, J. Acoust. Soc. Am. **75**, 35–45 (1984)], a spheroidal-coordinate-based transition matrix formalism was established for acoustic and elastic wave scattering. In this paper, the acoustic scattering by a solid elastic cylinder with hemispherical endcaps and a length-to-diameter ratio of 10 is considered. Numerical results are presented for the backscattered form function as a function of frequency for various angles of incidence. These results are compared with experimental measurements taken at the Naval Coastal Systems Center and given a physical interpretation.

PACS numbers: 43.20.Fn, 43.30.Gv

INTRODUCTION

In 1968, Waterman[1] introduced a new technique for systematically solving the acoustic diffraction problem for an arbitrarily shaped body, the transition matrix approach. For the sake of completenesss, we briefly outline the development of this formalism below. We assume that the acoustic field satisfies the standard Helmholtz equation

$$\phi^i(\mathbf{r}') + \int_s ds\, \hat{n}\cdot[\phi_+ \nabla G(k|\mathbf{r}-\mathbf{r}'|) - G(k|\mathbf{r}-\mathbf{r}'|)\nabla_+\phi] = \begin{cases}\phi(\mathbf{r}'), & r'\notin v,\\ 0, & r'\in v,\end{cases}$$

where ϕ is the total acoustic field, ϕ^i is the incident field, G is the free space Green's function and the integral is over the surface of the scatterer. The subscript $(+)$ denotes a boundary value as the surface is approached from its exterior and the two different values of the right-hand side of the equation refer to points exterior and interior to the scattering volume, v, respectively. We note that the latter case, i.e., when the field of the reradiating sources induced on the surface of the scatterer exactly cancels the incident field, is often referred to as the "extinction theorem."[2] Waterman's procedure is to expand the incident and scattered waves, ϕ^i and $\phi^s = \phi - \phi^i$, and the Green's function G, in regular and outgoing solutions to the scalar Helmholtz equation in spherical coordinates. Since the Green's function is singular when the source and field points coincide, for the extinction theorem the expansion procedure can be implemented only for field points which are interior to the largest sphere which can be inscribed in the scatterer and centered on the origin. However, ϕ is regular throughout the interior of the scatterer. Thus, by the process of analytic continuation, it follows that ϕ must vanish not just in the interior of the inscribing sphere, but throughout the interior of the scatterer. An infinite, coupled set of equations is developed from these results by expanding the unknown surface fields in a suitable basis set. A formal solution to this set of linear algebraic equations can be straightforwardly obtained, giving the expansion coefficients of the outgoing wave in terms of those of the incident field.

This procedure has a distinct advantage over competing approaches in that it appears to have the strongest theoretical foundation.[3–5] The approach is formally exact and computationally efficient (where applicable), and both the uniqueness[3] and the convergence[4,5] of the procedure can be proven for sound-soft and sound-hard scatterers for appropriate choices of basis functions. This is in marked contrast to the usual integral equation approach,[6] which leads to equations which are singular at certain discrete frequencies corresponding to the interior eigenvalue problem, and to those approaches embodying the *ad hoc* Rayleigh hypothesis.[7] The T-matrix formalism has been extended to elastic wave scattering by Waterman[8] and Pao and Varatharajulu[9] and to acoustic (i.e., scalar wave) scattering from an elastic target by Boström.[10]

It has been subsequently determined that this approach, although formally exact, suffers from a severe practical numerical limitation. For scatterers which deviate strongly from a spherical shape the number of terms required in the expansion of the surface fields increases dramatically and the matrices tend to become ill conditioned. This behavior had been predicted by Lewin,[11] who suggested that the source of this difficulty is a hypersensitivity of the surface field to minute errors of the field on the inscribed sphere. That is, assume that the extinction theorem is satisfied to a given order of approximation on the inscribed sphere with a given expansion. The further this spherical surface must be deformed to conform to the surface of the scatterer, the greater the error in the extrapolated value of the field and its derivatives on the surface and hence, the greater the induced error in the outgoing field.

Bates and Wall[12] were the first to suggest that these difficulties could be alleviated by formulating the scattering problem in alternative expansion functions which "better fit" the scatterer. These authors examined the efficacy of a two-dimensional elliptic-coordinate-based transition matrix for the scattering of scalar waves from large aspect ratio scatterers. They observed that choosing a coordinate system, such that the "radial coordinate = constant" surface lay as close to the surface of the scatterer as possible, alleviated the

ill-conditioning problems. In later work, Wall[13] attempted to develop a transition matrix in prolate spheroidal coordinates for vector wave scattering, but was unable to construct a Green's function expansion suitable for general waves. He did succeed in constructing a Green's function for axisymmetric waves,[14] and later applied this formalism to a cylindrical antenna problem.[15] While other authors[16–21] have suggested techniques for improving the numerical stability of the spherical-coordinate-based T matrix, none of these approaches holds the promise or the intuitive appeal of the spheroidal-coordinate-based formalism for large aspect ratio scatterers.

The difficulty in constructing a Green's function in spheroidal coordinates lies in the nonseparable nature of the vector Helmholtz equation in this coordinate system. As a consequence of this nonseparability, the vector wave functions are not orthogonal and the standard techniques for constructing the Green's function become intractable. Wall[14] succeeds in constructing an orthogonal set of spheroidal vector basis functions by considering grad(ψ) for the longitudinal degrees of freedom, and curl($\phi\chi$) for the transverse degrees of freedom, where ψ and χ are solutions to the scalar Helmholtz equation. However, he succeeds only at the cost of generality—as indicated above, these basis functions cannot describe off-axis scattering processes.

As Waterman has pointed out,[22] Huygen's principle is the fundamental concept underlying the T-matrix formalism, and the Green's function technique outlined above is simply one way of obtaining the T-matrix equations. Waterman[23] and Pao[24] have developed a simple alternative to the above development for displaying the mathematical content of Huygen's principle for vector waves in spherical coordinates. This technique is based on Betti's identity

$$\nabla\cdot[\vec{\sigma}(u)\cdot\mathbf{v} - \vec{\sigma}(v)\cdot\mathbf{u}] = 0,$$

where $\mathbf{u}$ and $\mathbf{v}$ are solutions to the vector Helmholtz equation and where $\vec{\sigma}$ is the associated stress tensor. In an earlier paper[25] (paper I), the covariant generalization of this technique was used to establish a transition matrix formalism for the scattering of general scalar or vector waves in prolate spheroidal coordinates. For vector waves, this approach is far more convenient than that originally adopted by Waterman, especially for coordinate systems in which the vector Helmholtz equation is not separable, as it obviates the need for constructing the vector Green's function. Thus the orthogonality of the vector basis states is no longer an important consideration. In the above work, the spheroidal vector basis functions were generated by considering grad(ψ) for the longitudinal degrees of freedom and curl($\mathbf{r}\chi$) for the transverse degrees of freedom. Here again, ψ and χ are solutions to the appropriate scalar Helmholtz equations. We shall refer to this choice of basis functions as the "standard" choice.[26] Like the standard spherical-coordinate-based approach, this formalism is suitable for scattering problems involving arbitrarily shaped bodies. Now however, we have the capability to explicitly tailor the formalism to the aspect ratio requirements of the scatterer. In the present paper, we consider a specific application of this approach to acoustic scattering from a finite, solid elastic cylinder to determine its efficiency in dealing with slender, elongated scatterers.

There have been a number of previous formulations of acoustic scattering problems in spheroidal coordinates. Kotani,[27] who is perhaps the earliest example, considered the acoustic diffraction by a circular disk in oblate spheroidal coordinates. Bowkamp,[28] and later Spence,[29] gave more thorough, rigorous treatments of this problem and of the diffraction by a circular aperture. Spence and Granger[30] are generally accredited with formulating the scattering from a rigid prolate spheroid as a modal harmonic sum in spheroidal coordinates. These authors presented numerical results in the form of beam patterns for various aspect ratios and angles of incidence for low frequencies. Senior[31] gave numerical results for rigid and pressure release spheroids for axially incident acoustic waves, and Klëschchev and Sheiba[32] extended these results to oblique incidence. There have been a number of solutions for the diffraction of plane waves in the high frequency regime.[33–37] The more predominant approach[33–36] has been to use an extension of the Watson transformation to convert the modal harmonic series for sound-hard and sound-soft spheroidal scatterers into a residue series which converges more rapidly at high frequencies. Lauchle,[37] however, directly evaluated the harmonic series by introducing high-frequency asymptotic expansions for the spheroidal functions.

Silbiger[38] was the first to consider the acoustic scattering by a penetrable spheroid in spheroidal coordinates. His treatment was incomplete in that the result was formulated in terms of a surface impedance operator Z, which is in general unknown. While Z was evaluated for several special cases, no attempt was made to incorporate the full complexity of an elastic prolate spheroidal scatterer. Yeh[39] considered the scattering from penetrable liquid (i.e., no shear degrees of freedom) prolate and oblate spheroids and gave numerical results for the special case that mode coupling is not present, i.e., when the sound speed of the scatterer is identical to that of water.

All of the above calculations involve only scalar fields and the boundary conditions can be implemented in a natural fashion due to the orthogonality of the solutions to the scalar Helmholtz equation in spheroidal coordinates. Formally, the acoustic scattering from elastic targets and the scattering of elastic waves (in elastic media) are far more difficult, as the transverse polarization degrees of freedom require the introduction of the prolate spheroidal vector wavefunctions. As a consequence of the nonorthogonality of the vector wavefunctions, the boundary conditions involving vector waves become relatively intractable in this coordinate system. Although a number of authors have dealt with elastic waves in spheroidal shells and solids,[40–45] it was not until after 1970 that the acoustic scattering from an elastic body was treated. In a series of papers, Grossman *et al.*,[46] Gutman and Klëshchev,[47] and Klëshchev[48] considered the acoustic scattering from a spheroidal elastic shell. These authors make the same choice for the vector basis set as the present author, in paper I.

To a considerable extent, the history of the formulation of electromagnetic scattering in spheroidal coordinates parallels that of the acoustic scattering problem. The earliest attempt was in 1927 by Möglich,[49] who considered the dif-

fraction of a plane polarized wave incident on a perfectly conducting circular disk. His treatment was incorrect, however, and the problem was not properly dealt with until 1948 by Meixner.[50] Meixner[51] and Flammer[52] later formulated the scattering of an electromagnetic wave by a conducting prolate spheroid in spheroidal coordinates for the special case that the source is a dipole oriented along the axis of the spheroid. Both of the above problems can be reduced to scalar form and the vector character of the electromagnetic wave need not be confronted. The more demanding problem of the scattering of a plane polarized electromagnetic wave by a conducting prolate spheroid, which required the use of the prolate spheroidal vector wavefunctions, was first formulated by Schultz,[53] for end-on incidence, and Rauch[54] extended this work to oblate spheroids. Siegel *et al.*[55-56] performed calculations based on Schultz's formalism and presented results for several (low) frequencies. These authors did not make the "standard" choice for the vector basis functions, i.e., that of paper I, but instead chose to represent the vector fields in rectangular coordinates with each of the components given a representation in terms of the solutions to the scalar Helmholtz equation. There was little further activity on this scattering problem until 1975, when Asano and Yamamoto[57] formulated the general problem of the scattering of a plane electromagnetic wave with an arbitrary angle of incidence on a dielectric spheroid. These authors' treatment of the problem differs from that of Schultz primarily in the use of the standard vector basis functions to represent the E and H fields. Numerical results were presented in the form of angular distributions for both oblate and prolate spheroidal scatterers for several different aspect ratios for low frequencies. In a subsequent series of papers, Asano,[58] Kotlarchyk *et al.*,[59] Asano and Sato,[60] and Asano[61] applied the model to an ensemble of randomly oriented scatterers.

This brief review would not be complete without mentioning the pioneering work of Van Buren *et al.*,[62] King *et al.*,[63] and King and Van Buren[64] on the generation of spheroidal functions, and the later improvements of Patz and Van Buren.[65] The availability of reliable, efficient codes for the calculation of the spheroidal functions has had a significant impact on the present work.

The first important result of the present work is the demonstration that the "standard" set of prolate spheroidal, vector basis functions is overcomplete. The $(\sigma,m,l)=(e,0,0)$, $\tau=1,2$ transverse vector basis states can be written as linear combinations of the remaining $(\sigma=e,m=0,l\neq 0)$ transverse vector basis states. It follows that all previous calculations utilizing these functions are suspect. This point is discussed further in Sec. I.

In Sec. II, we discuss the application of our approach to the acoustic scattering from elastic solids. To validate the theoretical procedures and computer codes, we have made a detailed experimental study of the acoustic scattering from a finite, 10:1 aluminum cylinder with hemispherical endcaps (Sec. III). Section IV is devoted to a comparison of the predictions of our approach with the experimental results and to an analysis of the elastic excitations underlying the more prominent features in the backscattered form function.

In Appendix A we give explicit expressions for the stress tensor in prolate spheroidal coordinates and in Appendix B, we derive the particular variant of the Moore–Penrose inverse used in the present work.

I. THE VECTOR BASIS FUNCTIONS

The prolate spheroidal, vector basis functions $\psi_{\tau n}$ used here were defined in paper I. We remind the reader that $\tau=1,2$ refers to transverse degrees of freedom, $\tau=3$, to the longitudinal degree of freedom, and that n refers to the set (σ,m,l) required to specify the particular solution to the scalar Helmholtz equation. In that paper, it was shown that these functions satisfy the relations

$$\oint_s ds\,[\mathbf{t}(\mathrm{Re}\,\psi_{\tau n})\cdot\mathrm{Re}\,\psi_{\tau' n'}-\mathbf{t}(\mathrm{Re}\,\psi_{\tau' n'})\cdot\mathrm{Re}\,\psi_{\tau n}]=0, \tag{1}$$

$$\oint_s ds\,[\mathbf{t}(\psi_{\tau n})\cdot\psi_{\tau' n'}-\mathbf{t}(\psi_{\tau' n'})\cdot\psi_{\tau n}]=0, \tag{2}$$

$$\oint_s ds\,[\mathbf{t}(\psi_{\tau n})\cdot\mathrm{Re}\,\psi_{\tau' n'}-\mathbf{t}(\mathrm{Re}\,\psi_{\tau' n'})\cdot\psi_{\tau n}]=i\delta_{\tau\tau'}\delta_{\sigma\sigma'}\delta_{mm'}O_{ll'}^{\tau m}, \tag{3}$$

where $O_{ll'}^{\tau m}$ is a real, symmetric matrix. In cases where the meaning will not be obscured, we shall drop the reference to τ.

These relations were used in conjunction with Betti's third identity to derive a mathematical representation of Huygen's principle, exterior to

$$-i\sum_n O_{n'n}a_{n'}=\oint_s ds\,[\mathbf{t}_+\cdot\psi_n-\mathbf{t}(\psi_n)\cdot\mathbf{u}_+], \tag{4}$$

$$i\sum_n O_{n'n}f_{n'}=\oint_s ds\,[\mathbf{t}_+\cdot\mathrm{Re}\,\psi_n-\mathbf{t}(\mathrm{Re}\,\psi_n)\cdot\mathbf{u}_+], \tag{5}$$

and interior to

$$0=\oint_s ds\,[\mathbf{t}_-\cdot\mathrm{Re}\,\psi_n^0-\mathbf{t}(\mathrm{Re}\,\psi_n^0)\cdot\mathbf{u}_-], \tag{6}$$

$$-i\sum_{n'}O_{n'n}^0 b_{n'}=\oint_s ds\,[\mathbf{t}_-\cdot\psi_n^0-\mathbf{t}(\psi_n^0)\cdot\mathbf{u}_-], \tag{7}$$

the scattering region. Here, $\{a_n\}$, $\{f_n\}$, and $\{b_n\}$ are the expansion coefficients of the incident, scattered, and refracted waves, and the superscript 0 denotes quantities pertaining to the scattering region. The $+(-)$ subscripts refer to boundary values taken at the exterior (interior) of the boundary of the scatterer, and s denotes that boundary.

The matrix $O_{ll'}^{\tau m}$ is the cornerstone of our approach and its detailed properties are of some interest. For $\tau=3$, $O_{ll'}^{\tau m}$ is diagonal in l and independent of m, i.e.,

$$O_{ll'}^{3m}=[(\lambda+2\mu)/k_L]\,\delta_{ll'}. \tag{8}$$

For the transverse degrees of freedom, $O_{ll'}^{\tau m}$ takes the form

$$O_{ll'}^{1m}=O_{ll'}^{2m}=(\mu/k_T)\Omega_{ll'}^{m}(h_T), \tag{9}$$

where $\Omega_{ll'}^{m}$ is a parity conserving angular integral which is easily calculable and may be expressed in terms of the expansion coefficients of the angular spheroidal functions. In the spherical limit ($f\to 0$, $\xi\to\infty$ with $f\xi\to kr$),

$$\lim_{h_T\to 0}\Omega_{ll'}^{m}(h_T)=\delta_{ll'}, \tag{10}$$

and Eq. (3) is simply an expression of the orthogonality of the vector spherical basis functions. In the present case, where h_T is, in general, nonzero and the functions are nonorthogonal, $O_{ll'}^{mm'}$ is nonetheless intimately involved with the linear independence of the basis functions $\{\psi_n\}$. That is, if

$$\mathbf{u} = \sum_n f_n \psi_n = 0, \tag{11}$$

then by Eq. (5), the necessary and sufficient condition for the vanishing of the $\{f_n\}$ is that $O_{ll'}^{mm'}$ be invertible.

We have examined the condition of $O_{ll'}^{mm'}$ by performing eigenvalue decomposition of $\Omega_{ll'}^{m}$ under varying levels of truncation of the expression[66]

$$\sum_{l'=0}^{N} \Omega_{ll'}^{m}(h_T) f_{\tau m l'} = 0, \tag{12}$$

with $\tau = 1,2$ and $0 < m < 15$. For sufficiently small values of N (the exact value depends upon h_T) the eigenvalues of Ω are positive and Ω is a well-conditioned matrix. As N increases, however, the smallest eigenvalue of $\Omega_{ll'}^{0}$ decreases to zero (to machine accuracy); that is, the $m = 0$ basis functions become linearly dependent. The remaining $\Omega_{ll'}^{m\neq 0}$ are well conditioned. As N is increased further (we have examined up to $N = 40$), the system remains stable in the sense that there is only a single eigenvalue consistent with zero. The remaining eigenvalues are positive and asymptotically approach unity with increasing order at a given level of truncation.

At small values of h_T, the null state of $O_{ll'}^{mm'}$ is predominantly $(\sigma,m,l) = (e,0,0)$. This perhaps could have been anticipated since this state vanishes identically in the spherical limit. While the l value of the largest component of the null state generally increases with h_T, there remains a significant $l = 0$ component throughout the range of h_T to be considered in this paper.

The ideal solution to this problem is to work with the eigenvectors of $O_{ll'}^{mm'}$ and remove the null state from consideration. The technique we adopt in Sec. II accomplishes this. We note, however, that as an alternative, we may simply remove the $l = 0$ transverse degrees of freedom. The resulting, truncated version of $O_{ll'}^{mm'}$ is well conditioned.

II. THEORETICAL CONSIDERATIONS

We begin by outlining the derivation of the spheroidal-coordinate-based transition matrix for the acoustic scattering from an elastic solid immersed in an inviscid fluid of infinite extent. We assume the usual boundary conditions

$$\hat{n}\cdot\mathbf{u}_+ = \hat{n}\cdot\mathbf{u}_-, \tag{13}$$

$$\hat{n}\cdot\mathbf{t}_+ = \hat{n}\cdot\mathbf{t}_-, \tag{14}$$

$$\hat{n}\times\mathbf{t}_- = 0, \tag{15}$$

apply at the surface of the scatterer. To account for the acoustic penetration of the scatterer, we introduce the expansion of the elastic displacement

$$\mathbf{u}^r = \sum_n b_n \operatorname{Re}\psi_n^0, \tag{16}$$

(the superscript 0 denotes quantities pertaining to the scatterer) and Eqs. (4) and (5) become

$$a_n = i\sum_{n'} R_{nn'} b_{n'}, \tag{17}$$

$$f_n = -i\sum_{n'} \hat{R}_{nn'} b_{n'}, \tag{18}$$

with

$$R_{nn'} = k/\lambda \oint_s ds\,[\hat{n}\cdot\mathbf{t}(\operatorname{Re}\psi_{n'}^0)\hat{n}\cdot\psi_n - \lambda\nabla\cdot\psi_n \hat{n}\cdot\operatorname{Re}\psi_{n'}^0], \tag{19}$$

$$\hat{R}_{nn'} = R_{nn'}(\psi_n \to \operatorname{Re}\psi_n). \tag{20}$$

To obtain a formal solution to Eqs. (17) and (18), we must now impose the $\hat{n}\times\mathbf{t} = 0$ boundary condition to reduce the number of degrees of freedom of the elastic field. It was shown by Boström[10] that this may be accomplished by using Eq. (6) to relate the elastic displacements, Eq. (16), to the acoustic nearfield displacements

$$\mathbf{u}_+ = \sum_n c_n \operatorname{Re}\psi_n. \tag{21}$$

The result is

$$\sum_{n'} P_{nn'} b_{n'} = \sum_{n'} M_{nn'} c_{n'}, \tag{22}$$

where

$$P_{nn'} = \oint_s ds\,[\hat{n}\cdot\mathbf{t}(\operatorname{Re}\psi_{n'}^0)\,\hat{n}\cdot\operatorname{Re}\psi_n^0 + \mathbf{t}(\operatorname{Re}\psi_n^0)\cdot\hat{n}\times(\hat{n}\times\operatorname{Re}\psi_{n'}^0)], \tag{23}$$

$$M_{nn'} = \oint_s ds\,\hat{n}\cdot\mathbf{t}(\operatorname{Re}\psi_n^0)\,\hat{n}\cdot\operatorname{Re}\psi_{n'}. \tag{24}$$

Combining the above results, we obtain the transition matrix

$$T = -\hat{Q}Q^{-1}, \tag{25}$$

$$Q = RP^{-1}M, \tag{26}$$

$$\hat{Q} = \hat{R}P^{-1}M. \tag{27}$$

Explicit expressions for the displacements and stress tensors required for the evaluation of P, M, and R in Eqs. (19), (20), (23), and (24) are given in paper I (displacements) and in Appendix A (stress tensors). We fix the interfocal distance $(2f)$ of our prolate spheroidal coordinate system for a particular scatterer by

$$f = [(\text{aspect ratio})^2 - 1]^{1/2}/(\text{aspect ratio}).$$

With this choice, the spheroid $\xi = 1/f$ exactly inscribes the scatterer.

The integrations in Eqs. (19), (20), (23), and (24) were performed using Gaussian quadrature. The matrix inversion implied in Eq. (25) was implemented by writing

$$Q^T T^T = -\hat{Q}^T, \tag{28}$$

(a superscript T denotes the matrix transpose) and then using Gauss elimination to solve for T^T, after scaling both Q and $\hat{Q}$. This procedure tends to be numerically more stable than a direct inversion of Q followed by matrix multiplication.

The remaining inversion

$$P^{-1}M,$$

in Eqs. (26) and (27) requires somewhat greater care. A de-

tailed examination of P for solid spheroids and finite cylinders with hemispherical endcaps reveals that this matrix tends to be ill conditioned. A typical eigenanalysis of P yields eigenvalues ranging in size from 10^{-26} to 10^{+2}. Holding the physical details of the scattering problem fixed, we find that the exact spectrum of eigenvalues depends upon the number of expansion terms. Invariably, however, after some level of truncation, increasing the number of terms in the expansion further merely tends to increase the number of eigenvalues roughly consistent with zero. The nonzero eigenvalues (and eigenvectors) are stable, to machine accuracy.

Interestingly enough, the stability of the calculation of the backscattered form function is to some extent, independent of the condition of P. For spheroidal bodies, the form function converges quite quickly and is stable under an almost arbitrarily large increase in the number of expansion terms. The finite cylinder displays a greater sensitivity to the condition of P and at high aspect ratios, when the condition of P has deteriorated sufficiently, the calculation becomes unstable. This latter behavior is probably due to the greater reliance of the cylindrical calculation on off-diagonal elements in P, M, and R.

There is a simple rationale for the relative insensitivity of T to the condition of P. Note that those elastic states which are weakly coupled to the nearfield can be no more than weakly coupled to the farfield. Thus, R and $\hat{R}$ must annihilate the same combinations of the expansion coefficients $\{b_n\}$ as P, and it follows that T is independent of the existence of these states. The difficulty with the finite cylinder is its greater reliance on off-diagonal matrix elements. In general, the far off-diagonal matrix elements are intrinsically less accurate than the diagonal elements and this annihilation process is not accurately performed.

Since it is presumably the presence of the uncoupled (or at most, weakly coupled) $\{b_n\}$ which is the source of the limited numerical stability for the finite cylinder, it should prove numerically advantageous to remove these states from our space. Defining Λ as the operator which projects into the space in which the matrix P is well defined, and using Λ to consistently obtain the admissible interior elastic states in Eqs. (17) through (24), we write Q in the form

$$Q = R\Lambda\,(\Lambda^{T}P\Lambda)^{-1}\Lambda^{T}M. \tag{29}$$

In Appendix B we give our procedure for constructing Λ and implementing the projection process in our calculations. The method is a variant of the Moore–Penrose pseudoinverse technique.[67] One immediate result of this projection procedure is that the T matrix (for the cylinder) becomes much more nearly symmetric. We find that $|T_{ll'} - T_{l'l}|$ is consistently smaller than 10^{-3} or 10^{-4} times the magnitude of the largest diagonal transition matrix element. There is essentially no effect on calculations for spheroidal bodies.

To compare our theoretical predictions with experimental measurements, we introduce the farfield form function with

$$f_{\infty}\left(\frac{kL}{2},\theta,\theta_0\right) = \lim_{r\to\infty}\frac{2r}{(L/2)}\left|\frac{p_s(kL/2,\theta,\theta_0)}{p_0}\right|, \tag{30}$$

where L is the length of the target, p_0 is the amplitude of the incident acoustic plane wave

$$p_0\,e^{ik\cdot r'} = 4\pi p_0\sum_{\sigma,m,l} i^{l}S_{\sigma ml}(h,\cos\theta_0,\phi_0) \times S_{\sigma ml}(h,\eta',\phi')\,je_{ml}(h,\xi'), \tag{31}$$

and p_s is the (angle-dependent) amplitude of the scattered wave

$$p_s(kL/2,\theta,\theta_0) = \sum_{\sigma,m,l} f_{\sigma ml}S_{\sigma ml}(h,\eta,\phi)\,he_{ml}(h,\xi),$$

$$f_{\sigma ml} = -4\pi P_0\sum_{l'} T^{\sigma m}_{ll'}\left(\frac{kL}{2}\right)i^{l'+1} \times S_{\sigma ml'}(h,\cos\theta_0,\phi_0). \tag{32}$$

Here, (θ_0,ϕ_0) and (θ,ϕ) are the spherical angles which define the direction of the incident and scattered waves, respectively, and the expansion coefficients of the scattered wave have been expressed in terms of the T matrix (T is diagonal in σ and m for axisymmetric objects). Explicitly introducing p_s and p_0 into Eq. (30) and utilizing the asymptotic $r\to\infty$ formula for he_{ml} gives

$$f_{\infty}\left(\frac{kL}{2},\theta,\theta_0\right) = \frac{8\pi}{(kL/2)}\left|\sum_{\sigma,m,l}(i)^{l'-l}S_{\sigma ml}(h,\cos\theta,\phi) \times T^{\sigma m}_{ll'}(kL/2)S_{\sigma ml'}(h,\cos\theta_0,\phi_0)\right|. \tag{33}$$

In general, we choose $\phi = \phi_0 = 0$. This definition is consistent with the general practice in the field and results in a form function of unity for a rigid spherical scatterer of radius $L/2$ in the high-frequency limit.

We have chosen to test our theoretical techniques against a finite cylindrical geometry for two reasons. First, the free waves which can propagate on a solid, infinite cylinder have been extensively studied and are well known.[68] Since a 10:1 cylinder is sufficiently long that the boundary conditions on the endcaps should not have an appreciable effect on these waves, this fact helps considerably in the analysis. In the present case, the only two contributing waves are (1) the lowest longitudinal mode, which can be characterized as an axially symmetric wave with displacement components only in the radial and axial directions, and (2) the lowest flexural mode, which in general depends upon all three directions. The dispersion curves for these waves are given in Fig. 1. The higher longitudinal and flexural modes have cutoff frequencies which are beyond the range considered here and the torsional modes cannot be excited acoustically.

Second, this geometry provides a more stringent test of the formalism than would a spheroid or a super spheroid. A spheroid is a special geometry for which both the spherical and spheroidal basis functions are very well suited. Boström[22] has noted that even small deviations from a spheroidal geometry leads to a significant deterioration in the numerical performance of the standard spherical-coodinate-based T matrix. In the next section we describe our experimental procedures.

III. EXPERIMENTAL

Backscattered acoustic waveforms were acquired from a 10:1 solid aluminum cylinder with hemispherical endcaps

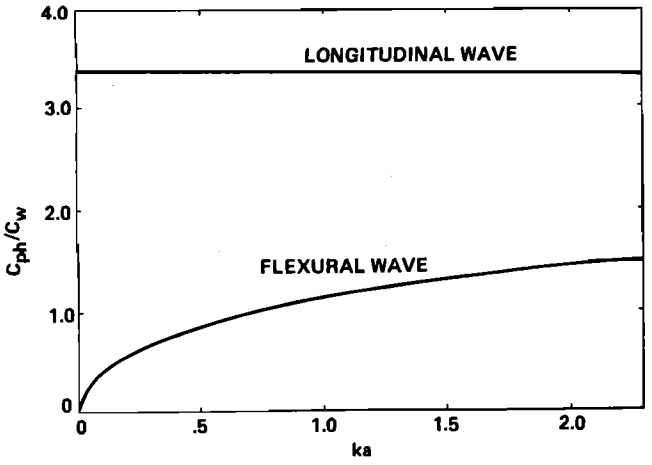

FIG. 1. The dispersion curves for the lowest longitudinal and flexural modes on an infinite aluminum cylinder of circular cross section.

as a function of aspect angle θ (the angle the acoustic axis makes with the long symmetry axis of the target). The experimental farfield form function was determined using the expression[69]

$$f_\infty\left(\frac{kL}{2},\theta\right)=\frac{2r}{L/2}\frac{g_s(kL/2,\theta)}{g_i(kL/2)},$$

where r is the distance from the center of the scattering target to the measurement point, $g_s(kL/2,\theta)$ is the transform of the backscattered waveform, $p_s(t)$, and $g_i(kL/2)$ is the transform of the incident pulse at the scattering target, $p_i(t)$.

Acoustic measurements were performed in a 10-×10-×7-ft reinforced concrete test pool filled with a suitable volume of freshwater as the acoustic medium. The source transducer, receive hydrophone, and scattering target were placed along a horizontal line, held by a system of precision positioning devices. Lateral, longitudinal, and vertical alignment of the components was accomplished optically using a sighting telescope. The respective positions were such as to maximize the shortest reverberant path, thus optimizing the time domain measurement window. A 6-in.-long target was selected based on the requirements that a sufficient backscattered return would be observed end on, and that a sufficient number of returns from surface waves traveling around the target would be acquired to yield a representative measure of the form function. This latter criteria was not fulfilled in certain cases, as will be discussed at the end of this section. The initial angular orientation (90° off axis) of the scattering target was determined acoustically by maximizing the backscattered signal. Throughout the measurements, the positions of the transducer and hydrophone remained fixed, while the aspect angle of the target was varied.

The relative pressure amplitudes $p_0(t)$ (of the incident waveform), and $p_s(t)$ were measured using a common hydrophone (B & K model 8203), placed in the farfield region of the transducer, a distance r from the scattering target. Appropriate corrections for spreading and absorption were made to yield an effective pressure wave front, $p_i(t)$, incident on the target. No attempt was made to correct for the slight distortion (estimated to be less than 1%) by the presence of a receiver hydrophone situated on a straight line between the source transducer and the scattering target.

The drive and receive electronics are depicted in Fig. 2. A single cycle sine wave, amplified by a power amplifier (Kronhite model DCA-50), provided the drive signal for the piezoelectric transducer (USRD type F-33). The acoustic signals received by the hydrophone were preamplified and bandpass filtered prior to digitizing by the HP-5180A waveform recorder.

Data acquisition was under the control of a HP-9826 microcomputer. Digitized representation of the analog waveforms was transferred to the microcomputer for off-line analysis. The data analysis routine allowed for signal averaging, convolution, and Fourier transformation of the digitized waveforms, along with graphic displays of the resultant operations. All recorded waveforms were repetitively averaged for 30 scans.

Waveforms were sampled and digitized such that the Nyquist rate was always exceeded. An 8192-point discrete fast Fourier transform was implemented with a rectangular window (no weighting) to obtain intermediate frequency domain data. In order to span the $kL/2$ region of interest (5–20), several different center frequencies were required. The 3-dB down points were chosen as the cutoff points for the contribution of each frequency band to the computed form function. In this context, we note that many of the form function plots represent averages of numerous independent measurements.

In viewing the individual backscattered waveforms for analysis, it became apparent that some of the returns persisted well beyond the available time window. The effect was particularly significant in regions where the theory predicted high Q resonant features. These observations were not surprising in that any experimental measurement has an inherent limitation on the resolution of such features. Assuming a decay modulus (time required for the amplitude to decrease to $1/e$ of its initial value) equal to the available

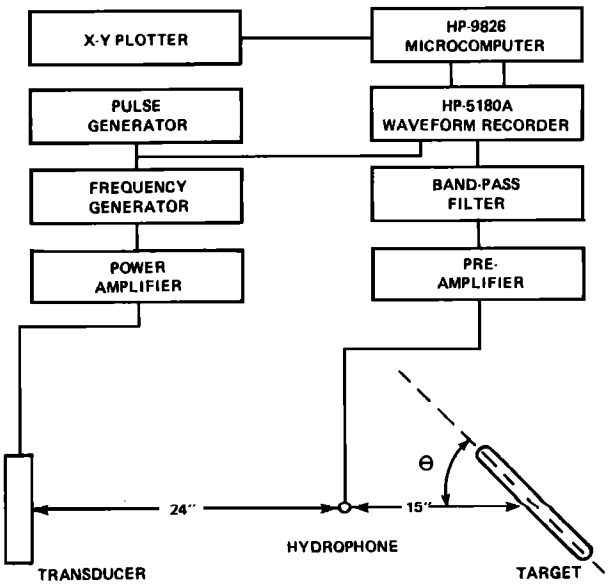

FIG. 2. A schematic representation of the experimental geometry and apparatus. Here, θ defines the experimental aspect angle.

window size (minus the specular return), we estimate that these measurements allow for the correct representation of features with a maximum Q value of five. The particular theoretical resonant features of interest clearly exceed this value.

In order to determine the effect such artificial termination had on the resultant form function, a simple subtraction was employed for the 30° off-axis measurement. Surface multipaths were removed by subtracting the multipath waveform (without target) from the backscattered target return. Although a residual signal was clearly present (giving rise to an interference pattern) and some of the signal still resided outside of the "expanded" measurement window, the agreement with theory was excellent, as will be discussed in the following section.

IV. DISCUSSION

A series of calculations of the monostatic backscattered form function was performed in the region $kL/2 < 20$ for comparison with experiment. There are two parameters to fix in the calculation of the $m = 0$ T matrix at a given frequency, the number of terms included in the truncation of the infinite dimensional matrix equations, $L_{\max}$ in Eqs. (25)–(27), and the number of significant figures retained in the orthogonalization of P, i.e., N_{orth} (see Appendix B). In the frequency range $kL/2 < 16$, the number of expansion terms was fixed by increasing $L_{\max}$ until the form function varied by 0.5% or less for a change $\Delta L_{\max} = 2$. The number of terms required for convergence with this criterion varied between ten at the low-frequency end and 30 at the upper frequencies. For $kL/2 > 16$, $L_{\max}$ was fixed at 30. We note that for $kL/2 \sim 20$, a change $\Delta L_{\max} = 2$ resulted in a change in the form function of less than 2%.

The calculation was relatively insensitive to the number of significant figures retained in the orthogonalization process, provided N_{orth} was sufficiently large, and we chose $N_{\text{orth}} = 18$–20. Increasing N_{orth} by two generally resulted in a change in the form function of much less than 0.5%.

No attempt was made to measure the density and sound speeds of the aluminum cylinder. Instead, the generic values $\rho = 2700$ kg/m^3, $C_l = 6420$ m/s, and $C_t = 3040$ m/s were used. Thus some discrepancy between the measured and calculated form function is expected due to the mismatch in the elastic parameters. To obtain some idea of the sensitivity of the calculation to reasonable variations in these parameters, we have examined the position of the lowest resonance for end-on incidence under a 10% variation in the Lame' parameter μ (the bar speed depends strongly on this parameter).[70] We find that the peak shifts by no more than 5%.

In Fig. 3 we exhibit a collection of calculated monostatic beam patterns which have been selected to display the more prominent features in the backscattered form function. In particular, the single, strong, high Q lobe at $\theta = 56°$ and $kL/2 = 5.4$ and the "ridge" of lobes with $\theta \simeq 30°$ beginning at $kL/2 = 6.6$ represent significant departures from rigid behavior. It is worth noting that with two exceptions, at $kL/2 = 5.4$ and 10.8, there is no ancillary structure (in the beam pattern) associated with these off-axis lobes. The two exceptions display on-axis resonances. We also note for future reference that the peak amplitude of the ridge, which has large, high Q peaks at $kL/2 = 6.7$, 9.3, and 12, shows a general tendency to move in the direction of increasing θ with increasing frequency. These features are particularly revealing

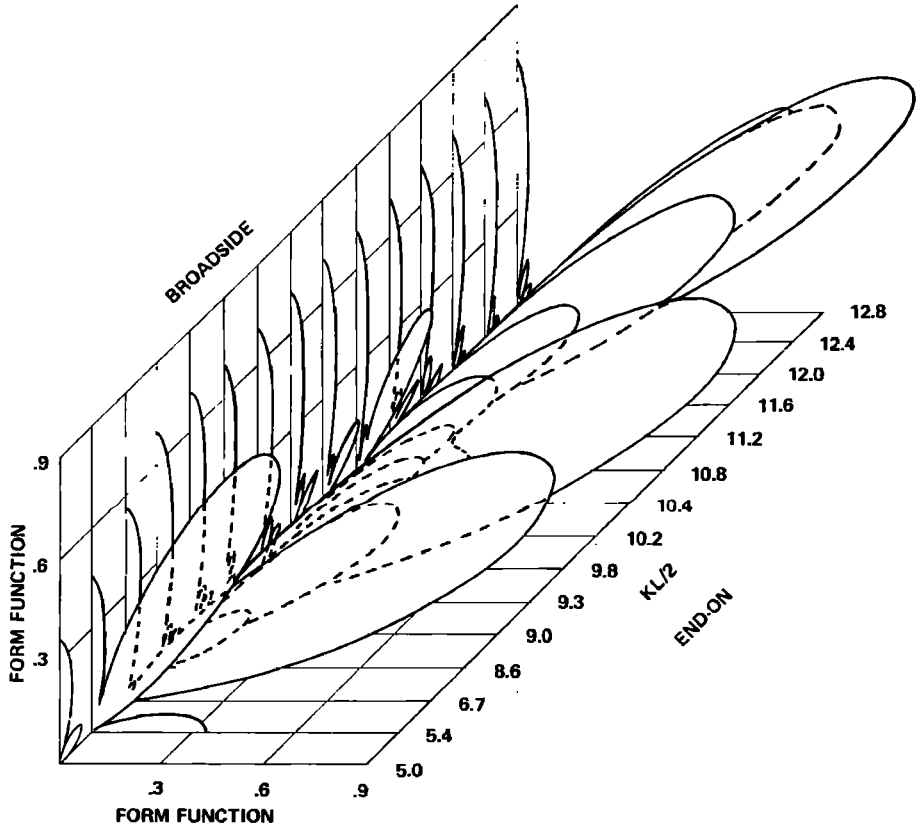

FIG. 3. The calculated monostatic beam patterns for a 10:1 finite aluminum cylinder with hemispherical endcaps.

of the elastic response of the scatterer and we shall explore this in detail below.

In Figs. 4 and 5, the calculated backscattered form function (solid points) is compared with the experimental data (solid lines) for aspect angles θ ranging from 0° to 90°, in 10° increments. In regions where the experimental frequency bands overlap, both sets of data are presented. The dashed lines in Fig. 5 for $\theta = 30°$, represent measurements taken with the expanded window discussed in the previous section. We note that the small scale oscillations in the data taken with the expanded window are an artifact of the subtraction procedure and do not have any underlying physical signficance. In this figure, it is clear that the longer window gives a considerable improvement in the agreement between the data and the calculations. It is also clear that the very high Q features in the calculation (e.g., at $kL/2 = 6.7$ and $\theta = 30°$) are still beyond the capabilities of the expanded window.

Consider first Fig. 4, i.e., end-on incidence. Since T-matrix calculations for end-on incidence require only the $m = 0$ term in Eq. (33) and thus tend to be less time consuming than off-axis orientations, a somewhat more ambitious calculational program was undertaken here than for more general angles of orientation; hence, the expanded frequency scale and greater density of points, as compared to Fig. 5. The signal strength from the target at this angle was too small to reliably subtract the multipaths so no attempt was made to obtain the high Q features present in the data. Given this qualification, the calculation is in reasonably good agreement with the data. The three peaks at $kL/2 = 5.4$, 10.8, and 16.2 are clearly the $\lambda = L/2$, L, and $3L/2$ resonances associated with the largely nondispersive, lowest longitudinal mode of an infinite elastic cylinder. We have examined the elastic displacements at the surface of the scatterer, and both the calculated phase speed and the displacements are in accord with this picture.

Consider next the prominent ridge of lobes in the backscattered form function depicted in Fig. 3 and in the $\theta = 30°$ portion of Fig. 5. This ridge is associated with the excitation of the lowest flexural wave of an infinite cylinder due to the matching of the trace velocity of the incident acoustic wave with the velocity of propagation of the flexural wave (see Fig. 2). An examination of the elastic displacements reveals that the three clearly identifiable resonance peaks at $\theta = 30°$ in Fig. 5 are associated with the $\lambda = 2L/5$, $L/3$, and $2L/7$ resonant wavelengths. The agreement of the calculation with the data, particularly that data obtained with the expanded window, is quite good. However, the very high Q portion of the resonance peaks is still missing. An examination of the time domain waveform shows that even with the expanded window, only a portion of the energy of these peaks has been captured, i.e., the waveform has been artificially and prematurely truncated. In the nonresonant region, the flexural wave is still excited, due to the strong coupling mechanism, and the elastic cylinder acts as a phase steered array, firing a highly directional and hence, strong signal back at the source. This mechanism also explains the surprising strength of the resonant response.

The single strong lobe at 56° (see the $\theta = 50°$ and $\theta = 60°$ aspect orientations in Fig. 5) is associated with the longitudinal (i.e., $m = 0$) response of the cylinder. An examination of the elastic displacements reveals a stationary longitudinal wave with $\lambda = L/2$ almost identical to that excited at end-on incidence at this frequency, but approximately 50% stronger. At this angle of incidence ($\theta = 56°$) and frequency, there is exactly one water wavelength along the projected length of the cylinder and it is the coherent shaking of the two ends which is responsible for the relatively strong excitation. Unfortunately, due to the very high Q nature of this lobe and the small signal strength, even with the expanded window only a small enhancement of the form function was observed at this angle. Therefore the data and calculations were not included in the figure.

Consider finally, the broadside form function. The frequency region considered here is too low for any significant elastic activity in the broadside or near broadside direction ($70° < \theta < 90°$). It is interesting to note that the off-axis behavior in this angular region differs markedly from that obtained in studies of the scattering of obliquely incident acoustic waves by an infinite cylinder by Flax *et al.*[71] However, the lobe structure in Fig. 3 in this angular region can be simply explained by treating a finite rigid cylinder of length L as a linear phase steered array excited by the incident acoustic wave. The primary, secondary, and tertiary lobes are all present and their position, angular width and relative magnitude are consistent with this simple picture, although the third lobe is somewhat larger than expected. We note that there is sufficient experimental sensitivity to the angular alignment in this region, due to the relatively narrow (in θ) lobes, to account for the small discrepancies between the data and calculations.

We note in closing that, in related work, Su *et al.*[72] and Numrich *et al.*[73] have compared with experiment the predictions of the standard, spherical-coordinate-based T matrix for a finite aluminum cylinder of small aspect ratio (2:1).

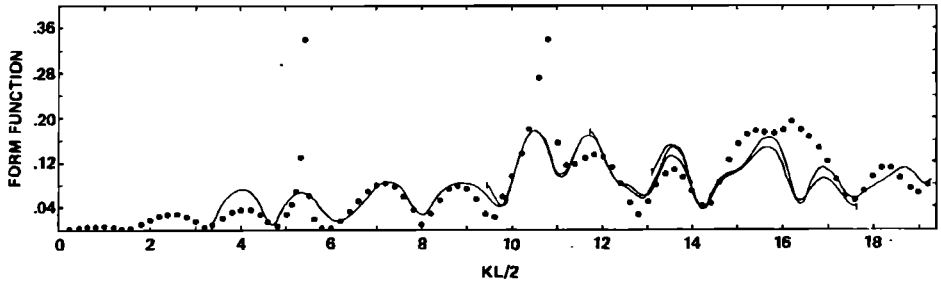

FIG. 4. The backscattered farfield form functions for a 10:1 finite aluminum cylinder with hemispherical endcaps for end-on incidence, plotted as a function of the dimensionless frequency $kL/2$. The heavy dots represent calculated values and the solid lines, experimental values. Note that in some regions, several frequency bands overlap.

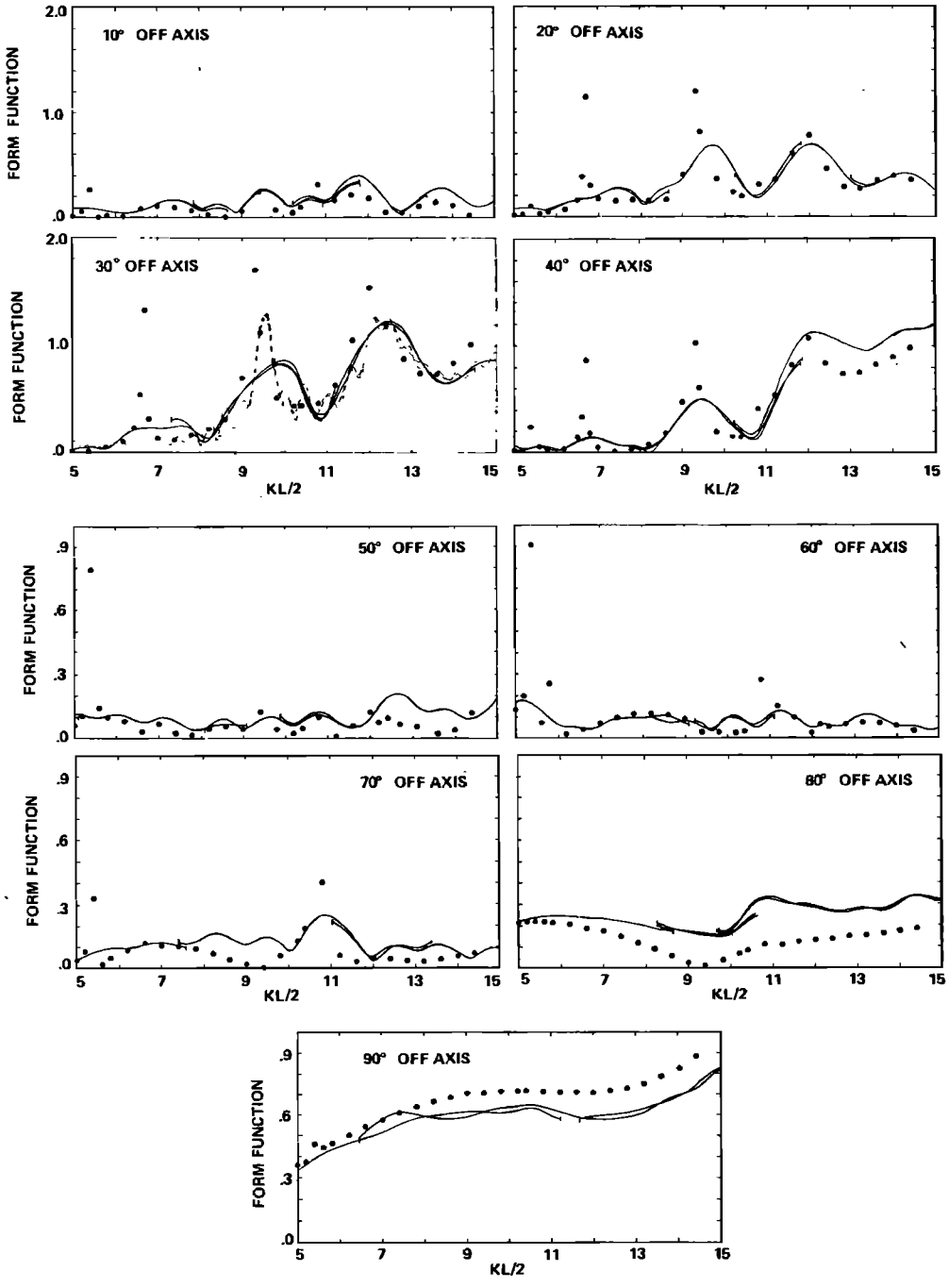

FIG. 5. The backscattered farfield form function for a 10:1 finite aluminum cylinder with hemispherical endcaps for off-axis incidence. The notation is the same as in Fig. 4. The additional dashed lines in the $\theta = 30°$ graph represent experimental values obtained with the expanded window as discussed in Sec. IV.

ACKNOWLEDGMENTS

The authors are indebted to D. H. Trivett for stimulating and productive conversations throughout the course of this work. One of us (RHH) would also like to thank A. L. Van Buren for discussions pertaining to the generation of the prolate spheroidal functions and for copies of his spheroidal function codes. In particular, the elegant eigenvalue routine of Patz and Van Buren[65] served as the heart of our eigenfunction routine. RHH would also like to thank J. Dobeck for discussions on the Moore–Penrose pseudoinverse and T. Rackers for producing the dispersion curves in the text. Finally, the authors would like to thank L. Flax for his continued encouragement and support.

APPENDIX A

In applications of the spheroidal-coordinate-based transition matrix, it is necessary to have explicit expressions for the vector basis functions and their associated stress tensors. Expressions for the basis functions were given in paper I; we give the stress tensors in this Appendix.

Following Morse and Feshbach,[74] we introduce the independent variables

$$(x_1,x_2,x_3) = (\xi,\eta,\cos\phi). \tag{A1}$$

The associated unit vectors

$$\hat{a}_1 = \hat{\xi}, \quad \hat{a}_2 = \hat{\eta}, \quad \hat{a}_3 = \cos\hat{\phi} = -\hat{\phi} \tag{A2}$$

define a right-handed coordinate system. This differs from the definitions adopted in paper I which utilized a left-handed coordinate system. Thus, there are several minus sign differences between the vector basis functions given in paper I and those adopted here, and these differences are noted in Eq. (A4). For calculational purposes, it is convenient to work with a representation of the vector basis functions in which the "physical" components are utilized, i.e.,

$$\psi_{\tau n} = \sum_{i=1}^{3} (\tilde{\psi}_{\tau n})_i \hat{a}_i. \tag{A3}$$

The relation between these physical components and the covariant expressions given in paper I [the $(\psi_{\tau n})_\alpha$], is

$$\begin{aligned}
(\tilde{\psi}_{\tau n})_1 &= \pm (h_1)^{-1} (\psi_{\tau n})_1, \\
(\tilde{\psi}_{\tau n})_2 &= \mp (h_2)^{-1} (\psi_{\tau n})_2, \\
(\tilde{\psi}_{\tau n})_3 &= \pm (h_3)^{-1} (\psi_{\tau n})_3,
\end{aligned} \tag{A4}$$

where the upper sign is for $\tau = 1, 3$ and the lower, for $\tau = 2$. The h_i denote the scale factors

$$\begin{aligned}
h_1 &= f[(\xi^2 - \eta^2)/(\xi^2 - 1)]^{1/2}, \\
h_2 &= f[(\xi^2 - \eta^2)/(1 - \eta^2)]^{1/2}, \\
h_3 &= (f/\sin\phi)[(1 - \eta^2)(\xi^2 - 1)]^{1/2}.
\end{aligned} \tag{A5}$$

The stress tensor is defined by

$$\vec{\sigma}(\psi_{\tau n}) = \lambda \nabla \cdot \psi_{\tau n} \vec{1} + \mu(\nabla \psi_{\tau n} + \psi_{\tau n} \nabla), \tag{A6}$$

where

$$\vec{1} = \hat{a}_1 \hat{a}_1 + \hat{a}_2 \hat{a}_2 + \hat{a}_3 \hat{a}_3$$

is the unit dyadic and where

$$\begin{aligned}
\nabla \psi_{\tau n} + \psi_{\tau n} \nabla &= 2 \sum_i \left[\frac{\partial}{\partial x_i} \left(\frac{(\tilde{\psi}_{\tau n})_i}{h_i} \right) + \psi_{\tau n} \cdot \nabla (1 n\, h_i) \right] \hat{a}_i \hat{a}_i \\
&\quad + \sum_{i<j} \left[\frac{h_i}{h_j} \frac{\partial}{\partial x_j} \left(\frac{(\tilde{\psi}_{\tau n})_i}{h_i} \right) + \frac{h_j}{h_i} \frac{\partial}{\partial x_i} \left(\frac{(\tilde{\psi}_{\tau n})_j}{h_j} \right) \right] \\
&\quad \times (\hat{a}_i \hat{a}_j + \hat{a}_j \hat{a}_i).
\end{aligned} \tag{A7}$$

Let $\chi_n = R_{ml}(h_T, \xi) S_{oml}(h_T, \eta, \phi)$ denote a properly normalized solution to the scalar Helmholtz equation with $k = k_T$, and let $A_{ml} = A_{ml}(h_T)$ denote the eigenvalue. For the transverse degrees of freedom, the physical components of the stress tensor (σ_{ij}) are given by

$$A_{ml}^{1/2} \sigma(\psi_{1n})_{11} = \frac{2\mu}{f} \frac{1}{(\xi^2 - \eta^2)} \left(\eta \frac{\partial^2}{\partial \xi \partial \phi} \chi_n - \frac{\eta \xi}{(\xi^2 - 1)} \frac{\partial}{\partial \phi} \chi_n \right), \tag{A8}$$

$$A_{ml}^{1/2} \sigma(\psi_{1n})_{12} = \frac{\mu}{f} \frac{1}{[(1 - \eta^2)(\xi^2 - 1)]^{1/2}} \frac{1}{(\xi^2 - \eta^2)} \left((\xi^2 + \eta^2) \frac{\partial}{\partial \phi} \chi_n + \eta(1 - \eta^2) \frac{\partial^2}{\partial \eta \partial \phi} \chi_n - \xi(\xi^2 - 1) \frac{\partial^2}{\partial \xi \partial \phi} \chi_n \right), \tag{A9}$$

$$A_{ml}^{1/2} \sigma(\psi_{1n})_{22} = \frac{-2\mu}{f} \frac{1}{(\xi^2 - \eta^2)} \left(\xi \frac{\partial^2}{\partial \eta \partial \phi} \chi_n + \frac{\eta \xi}{(1 - \eta^2)} \frac{\partial}{\partial \phi} \chi_n \right), \tag{A10}$$

$$\begin{aligned}
A_{ml}^{1/2} \sigma(\psi_{1n})_{13} &= \frac{\mu}{f} \frac{1}{[(1 - \eta^2)(\xi^2 - \eta^2)]^{1/2}} \frac{1 - \eta^2}{\xi^2 - \mu^2} \Big[-2\eta\xi \frac{\partial}{\partial \xi} \chi_n - \xi(\xi^2 - 1) \frac{\partial^2}{\partial \xi \partial \eta} \chi_n \\
&\quad + \eta \Big((A_{ml} - h_T^2 \xi^2) + m^2 \frac{(\xi^2 + 1 - 2\eta^2)}{(\xi^2 - 1)(1 - \eta^2)} \Big) \chi_n - (\xi^2 - 1) \frac{\partial}{\partial \eta} \chi_n - 2 \frac{\xi(\xi^2 - 1)}{(\xi^2 - \eta^2)} \left(\eta \frac{\partial}{\partial \xi} \chi_n - \xi \frac{\partial}{\partial \eta} \chi_n \right) \Big],
\end{aligned} \tag{A11}$$

$$\begin{aligned}
A_{ml}^{1/2} \sigma(\psi_{1n})_{23} &= \frac{\mu}{f} \frac{1}{[(\xi^2 - 1)(\xi^2 - \eta^2)]^{1/2}} \frac{\xi^2 - 1}{\xi^2 - \eta^2} \Big[-2\eta\xi \frac{\partial}{\partial \eta} \chi_n + \eta(1 - \eta^2) \frac{\partial^2}{\partial \xi \partial \eta} \chi_n \\
&\quad + \xi \left((A_{ml} - h_T^2 \eta^2) - m^2 \frac{(2\xi^2 - 1 - \eta^2)}{(1 - \eta^2)(\xi^2 - 1)} \right) \chi_n + (1 - \eta^2) \frac{\partial}{\partial \xi} \chi_n + 2 \frac{\eta(1 - \eta^2)}{(\xi^2 - \eta^2)} \left(\eta \frac{\partial}{\partial \xi} \chi_n - \xi \frac{\partial}{\partial \eta} \chi_n \right) \Big],
\end{aligned} \tag{A12}$$

and

$$\begin{aligned}
k_T A_{ml}^{1/2} \sigma(\psi_{2n})_{11} &= \frac{2\mu}{f^2} \Big\{ -\frac{1}{(\xi^2 - \eta^2)} \xi \frac{\partial}{\partial \xi} \chi_n + \frac{1}{(\xi^2 - \eta^2)^2} \Big[(A_{ml} - h_T^2 \xi^2) \left(\eta(1 - \eta^2) \frac{\partial}{\partial \eta} \chi_n + (1 - 3\eta^2) \chi_n \right) \\
&\quad + (A_{ml} - h_T^2 \eta^2) \left(\xi(\xi^2 - 1) \frac{\partial}{\partial \xi} \chi_n + (3\xi^2 - 1) \chi_n \right) + 2\xi(\xi^2 - 1) \frac{\partial}{\partial \xi} \chi_n \\
&\quad - \xi^2 (A_{ml} - h_T^2 \eta^2) \chi_n - \eta\xi(1 - \eta^2) \frac{\partial^2}{\partial \eta \partial \xi} \chi_n \Big] + \frac{1}{(\xi^2 - \eta^2)^3} \Big[[3\eta^2(1 - \eta^2)(A_{ml} - h_T^2 \xi^2) \\
&\quad - 3\xi^2(\xi^2 - 1)(A_{ml} - h_T^2 \eta^2)] \chi_n - (7\xi^2 - 3) \left(\eta(1 - \eta^2) \frac{\partial}{\partial \eta} \chi_n + \xi(\xi^2 - 1) \frac{\partial}{\partial \xi} \chi_n \right) \\
&\quad - 6\xi(\xi^2 - 1)^2 \frac{\partial}{\partial \xi} \chi_n - 6\eta\xi(\xi^2 - 1)(1 - \eta^2) \frac{\partial^2}{\partial \xi \partial \eta} \chi_n \Big] + \frac{1}{(\xi^2 - \eta^2)^4} \Big[12\xi^2(\xi^2 - 1) \\
&\quad \times \left(\eta(1 - \eta^2) \frac{\partial}{\partial \eta} \chi_n + \xi(\xi^2 - 1) \frac{\partial}{\partial \xi} \chi_n \right) \Big] + m^2 \Big[\frac{1}{(\xi^2 - \eta^2)^2} \left(\frac{-\eta^2}{\xi^2 - 1} - 3 \frac{(\xi^2 + \eta^2)}{(\xi^2 - \eta^2)} \right) \chi_n \\
&\quad + \frac{1}{(\xi^2 - 1)(\xi^2 - \eta^2)^2} \left(\eta(1 - \eta^2) \frac{\partial}{\partial \eta} \chi_n + \xi(\xi^2 - 1) \frac{\partial}{\partial \xi} \chi_n \right) \Big] \Big],
\end{aligned} \tag{A13}$$

$$k_T A_{ml}^{1/2}\sigma(\psi_{2n})_{22}=\frac{2\mu}{f^2}\left\{\frac{1}{(\xi^2-\eta^2)}\eta\frac{\partial}{\partial\eta}\chi_n+\frac{1}{(\xi^2-\eta^2)^2}\left[-(A_{ml}-h_T^2\eta^2)\left(\xi(\xi^2-1)\frac{\partial}{\partial\xi}\chi_n+(3\xi^2-1)\chi_n\right)\right.\right.$$
$$-(A_{ml}-h_T^2\xi^2)\left(\eta(1-\eta^2)\frac{\partial}{\partial\eta}\chi_n+(1-3\eta^2)\chi_n\right)-2\eta(1-\eta^2)\frac{\partial}{\partial\eta}\chi_n$$
$$-\eta^2(A_{ml}-h_T^2\xi^2)\chi_n+\eta\xi(\xi^2-1)\frac{\partial^2}{\partial\xi\partial\eta}\chi_n\Big]+\frac{1}{(\xi^2-\eta^2)^3}\Big[[3\xi^2(\xi^2-1)(A_{ml}-h_T^2\eta^2)$$
$$-3\eta^2(1-\eta^2)(A_{ml}-h_T^2\xi^2)]\chi_n-(7\eta^2-3)\left(\xi(\xi^2-1)\frac{\partial}{\partial\xi}\chi_n+\eta(1-\eta^2)\frac{\partial}{\partial\eta}\chi_n\right)$$
$$+6\eta(1-\eta^2)^2\frac{\partial}{\partial\eta}\chi_n+6\eta\xi(1-\eta^2)(\xi^2-1)\frac{\partial^2}{\partial\eta\partial\xi}\chi_n\Big]+\frac{1}{(\xi^2-\eta^2)^4}\Big[12\eta^2(1-\eta^2)\Big(\xi(\xi^2-1)\frac{\partial}{\partial\xi}\chi_n$$
$$+\eta(1-\eta^2)\frac{\partial}{\partial\eta}\chi_n\Big)\Big]+m^2\left[\frac{1}{(\xi^2-\eta^2)^2}\left(\frac{\xi^2}{1-\eta^2}+3\frac{(\xi^2+\eta^2)}{(\xi^2-\eta^2)}\right)\chi_n+\frac{1}{(1-\eta^2)(\xi^2-\eta^2)^2}\right.$$
$$\left.\left.\times\left(\xi(\xi^2-1)\frac{\partial}{\partial\xi}\chi_n+\eta(1-\eta^2)\frac{\partial}{\partial\eta}\chi_n\right)\right]\right\}, \tag{A14}$$

$$k_T A_{ml}^{1/2}\sigma(\psi_{2n})_{12}=\frac{2\mu}{f^2}[(\xi^2-1)(1-\eta^2)]^{1/2}\left\{-\frac{1}{\xi^2-\eta^2}\frac{\partial^2}{\partial\xi\partial\eta}\chi_n+\frac{1}{(\xi^2-\eta^2)^2}\left[3(2\xi^2-1)\frac{\partial^2}{\partial\xi\partial\eta}\chi_n\right.\right.$$
$$\left.+\left(A_{ml}-\frac{h_T^2}{2}(\xi^2+\eta^2)+3\right)\left(\xi\frac{\partial}{\partial\eta}\chi_n-\eta\frac{\partial}{\partial\xi}\chi_n\right)\right]+\frac{1}{(\xi^2+\eta^2)^3}\Big[-6\xi^2(\xi^2-1)\frac{\partial^2}{\partial\xi\partial\eta}\chi_n$$
$$+6\eta\xi\left(A_{ml}-\frac{h_T^2}{2}(\xi^2+\eta^2)\right)\chi_n-\xi(10\xi^2-\eta^2-3)\frac{\partial}{\partial\eta}\chi_n-\eta(10\eta^2-\xi^2-3)\frac{\partial}{\partial\xi}\chi_n\Big]$$
$$+\frac{1}{(\xi^2-\eta^2)^4}\left[6[\xi^2(\xi^2-1)-\eta^2(1-\eta^2)]\left(\xi\frac{\partial}{\partial\eta}\chi_n-\eta\frac{\partial}{\partial\xi}\chi_n\right)\right]$$
$$\left.+m^2\left[\frac{3\eta\xi}{(\xi^2-\eta^2)^3}\left(\frac{1}{\xi^2-1}-\frac{1}{1-\eta^2}\right)\chi_n+\frac{1}{(\xi^2-\eta^2)^2}\left(\frac{\xi}{\xi^2-1}\frac{\partial}{\partial\eta}\chi_n+\frac{\eta}{1-\eta^2}\frac{\partial}{\partial\xi}\chi_n\right)\right]\right\}, \tag{A15}$$

$$k_T A_{ml}^{1/2}\sigma(\psi_{2n})_{13}=-\frac{2\mu}{f^2}\frac{1}{[(1-\eta^2)(\xi^2-\eta^2)]^{1/2}}\frac{1}{\xi^2-\eta^2}\left\{\xi\left[\left(A_{ml}-\frac{1}{2}h_T^2(\xi^2+\eta^2)\right)-\frac{\xi^2-\eta^2}{\xi^2-1}+\frac{m^2}{\xi^2-1}\right]\frac{\partial}{\partial\phi}\chi_n\right.$$
$$-\left(\eta^2+\frac{(\xi^2-1)(\xi^2+\eta^2)}{\xi^2-\eta^2}\right)\frac{\partial^2}{\partial\xi\partial\phi}\chi_n-\eta\xi\frac{(1-\eta^2)(3\xi^2-2-\eta^2)}{(\xi^2-1)(\xi^2-\eta^2)}\frac{\partial^2}{\partial\eta\partial\phi}\chi_n$$
$$\left.+\eta(1-\eta^2)\frac{\partial^3}{\partial\xi\partial\eta\partial\phi}\chi_n\right\}, \tag{A16}$$

$$k_T A_{ml}^{1/2}\sigma(\psi_{2n})_{23}=\frac{2\mu}{f^2}\frac{1}{[(\xi^2-1)(\xi^2-\eta^2)]^{1/2}}\frac{1}{\xi^2-\eta^2}\left\{\eta\left[\left(A_{ml}-\frac{1}{2}h_T^2(\xi^2+\eta^2)\right)-\frac{\xi^2-\eta^2}{1-\eta^2}-\frac{m^2}{1-\eta^2}\right]\frac{\partial}{\partial\phi}\chi_n\right.$$
$$-\left(\xi^2+\frac{(1-\eta^2)(\xi^2+\eta^2)}{\xi^2-\eta^2}\right)\frac{\partial^2}{\partial\eta\partial\phi}\chi_n-\eta\xi\frac{(\xi^2-1)(\xi^2+2-3\eta^2)}{(1-\eta^2)(\xi^2-\eta^2)}\frac{\partial^2}{\partial\xi\partial\phi}\chi_n$$
$$\left.-\xi(\xi^2-1)\frac{\partial^3}{\partial\xi\partial\eta\partial\phi}\chi_n\right\}. \tag{A17}$$

In the above expressions, we have eliminated all reference to $\partial^2\chi/\partial\xi^2$, $\partial^2\chi/\partial\eta^2$, and $\partial^2\chi/\partial\phi^2$ through the use of the defining differential equations for R_{ml} and S_{oml}.

Using $\phi_n=R_{ml}(h_L,\xi)S_{oml}(h_L,\eta,\phi)$ to denote a properly normalized solution to the scalar Helmholtz equation with $k=k_L$, and $A_{ml}=A_{ml}(h_L)$ to denote the eigenvalue, for the irrotational degree of freedom, we find

$$k_L\sigma(\psi_{3n})_{11}=-k_L^2\lambda\phi_n+\frac{2\mu}{f^2}\left[\frac{1}{\xi^2-\eta^2}\left((A_{ml}-h_L^2\xi^2)\phi_n-\xi\frac{\partial}{\partial\xi}\phi_n\right)-\frac{1}{(\xi^2-\eta^2)^2}\right.$$
$$\left.\times\left(\xi(\xi^2-1)\frac{\partial}{\partial\xi}\phi_n+\eta(1-\eta^2)\frac{\partial}{\partial\eta}\phi_n\right)+m^2\frac{1}{(\xi^2-1)(\xi^2-\eta^2)}\phi_n\right], \tag{A18}$$

$$k_L\sigma(\psi_{3n})_{12}=\frac{2\mu}{f^2}[(1-\eta^2)(\xi^2-1)]^{1/2}\left[\frac{1}{\xi^2-\eta^2}\frac{\partial^2}{\partial\xi\partial\eta}\phi_n+\frac{1}{(\xi^2-\eta^2)^2}\left(\eta\frac{\partial}{\partial\xi}\phi_n-\xi\frac{\partial}{\partial\eta}\phi_n\right)\right], \tag{A19}$$

$$k_L\sigma(\psi_{3n})_{22} = -k_L^2\lambda\phi_n + \frac{2\mu}{f^2}\left[-\frac{1}{\xi^2-\eta^2}\left((A_{ml}-h_L^2\eta^2)\phi_n - \eta\frac{\partial}{\partial\eta}\phi_n\right)\right.$$
$$\left. + \frac{1}{(\xi^2-\eta^2)^2}\left(\xi(\xi^2-1)\frac{\partial}{\partial\xi}\phi_n + \eta(1-\eta^2)\frac{\partial}{\partial\eta}\phi_n\right) + m^2\frac{1}{(1-\eta^2)(\xi^2-\eta^2)}\phi_n\right], \tag{A20}$$

$$k_L\sigma(\psi_{3n})_{13} = -\frac{2\mu}{f^2}\frac{1}{[(1-\eta^2)(\xi^2-\eta^2)]^{1/2}}\left(\frac{\partial^2}{\partial\phi\partial\xi}\phi_n - \frac{\xi}{\xi^2-1}\frac{\partial}{\partial\phi}\phi_n\right), \tag{A21}$$

$$k_L\sigma(\psi_{3n})_{23} = -\frac{2\mu}{f^2}\frac{1}{[(\xi^2-1)(\xi^2-\eta^2)]^{1/2}}\left(\frac{\partial^2}{\partial\phi\partial\eta}\phi_n - \frac{\eta}{1-\eta^2}\frac{\partial}{\partial\phi}\phi_n\right). \tag{A22}$$

APPENDIX B

Consider the ill-conditioned problem

$$PC = M, \tag{B1}$$

where C and M are $n\times m$ rectangular matrices and where P is an $n\times n$ real, symmetric matrix with one or more zero eigenvalues. Here, C is to be determined. Let λ_k be the k th eigenvalue of P and let $p_i(k)$ be the corresponding normalized eigenvector, i.e.,

$$\sum_j P_{ij}\,p_j(k) = \lambda_k\,p_i(k). \tag{B2}$$

Then the transformation matrix which diagonalizes P is

$$U_{ij} = p_i(j). \tag{B3}$$

We assume that P has N nonzero eigenvalues, and that these eigenvalues are ordered by decreasing magnitude. The inconsistencies may be removed from Eq. (B1) by eliminating the null space of P. This is most straightforwardly accomplished by performing an eigenvalue decomposition of P and projecting into the space spanned by eigenvectors having nonzero eigenvalues; that is, we wish to cast Eq. (B1) into the form

$$\Omega_N\,U_N^T\,C = U_N^T\,M, \tag{B4}$$

where

$$\Omega_N = \begin{pmatrix}\lambda_1 & & & \\ & \lambda_2 & & 0 \\ & & \ddots & \\ & 0 & & \lambda_N\end{pmatrix}, \tag{B5}$$

$$|\lambda_n| > 0, \quad n = 1,\ldots,N,$$

and where U_N is the truncated diagonalization transformation matrix. However, the explicit construction of the eigenvalues and eigenvectors tends to be time consuming, and we adopt a somewhat different procedure here.

From the spectral decomposition

$$P_{ij} = \sum_{k=1}^{n}\lambda_k\,p_i(k)\,p_j(k), \tag{B6}$$

it is clear that if P is of rank N, then P has exactly N linearly independent columns. To form a basis for this N-dimensional space, we apply the modified Graham–Schmidt orthogonalization procedure to the columns of P, with pivoting. That is, at each step in the orthogonalization procedure, from among the non-normalized columns of P, we choose the column with the largest norm, normalize it and orthogonalize all of the remaining columns relative to this choice. Clearly, this procedure can be applied only N times before we have exhausted the possibilities. In practice, we orthogonalize all columns, then order the columns by their loss of significant digits (through the subtraction process) and truncate at the point where more than 18 significant figures have been lost.

The columns of the $n\times N$ matrix Λ thus formed, must be a linear combination of the eigenvectors having $|\lambda_k| > 0$, i.e.,

$$\Lambda_{ij} = \sum_{k=1}^{N} p_i(k)\,A_{kj} \tag{B7}$$

which in matrix notation is

$$\Lambda = U_N\,A. \tag{B8}$$

From the orthonormality of the columns of Λ it follows that the $N\times N$ matrix A is orthogonal. From Eq. (B8), we thus have

$$U_N = \Lambda\,A^T. \tag{B9}$$

Returning to Eq. (B4) and utilizing

$$\Lambda^T P\Lambda = A^T\Omega_N\,A \tag{B10}$$

we find

$$(\Lambda^T P\Lambda)\Lambda^T C = \Lambda^T M, \tag{B11}$$

i.e., that Λ performs the necessary projection process. Note that it is not necessary to construct A.

The exact relation between the loss of significant digits in the columns of P during the orthogonalization process and the size of the magnitudes of the eigenvalues in Ω_N is unclear. This is unimportant, however, since our real concern is the linear independence of the columns (and rows) of the truncated matrix.

[1] P. C. Waterman, "New Formulation of Acoustic Scattering," J. Acoust. Soc. Am. **45**, 1471–1429 (1969).

[2] This terminology is most generally accredited to C. W. Oseen, Ann. Phys. **48**, 1 (1915); and P. P. Ewald, Ann. Phys. **49**, 1 (1916).

[3] P. A. Martin, "On the Null-Field Equations for the Exterior Problems of Acoustics," Q. J. Mech. Appl. Math. XXXIII, 385–396 (1980); P. A. Martin, "Acoustic Scattering and Radiation Problems and the Null-Field Method," Wave Motion **4**, 391–408 (1982).

[4] A. G. Ram, "Convergence of the T-Matrix Approach to Scattering Theory," J. Math. Phys. **23**, 1123–1125 (1982).

[5] G. Kristensson, A. G. Ramm, and S. Strom, "Convergence of the T-Matrix Approach in Scattering Theory II," J. Math. Phys. **24**, 2619–2631 (1983).

[6] For recent work utilizing this technique, see W. Tobocman, "Calculation of Acoustic Wave Scattering by Means of Helmholtz Integral Equation. I," J. Acoust. Soc. Am. **76**, 599–607 (1984); W. Tobocman, "Calculation of Acoustic Wave Scattering by Means of the Helmholtz Integral Equation.

II," J. Acoust. Soc. Am. 76, 1549–1554; W. Tobocman, "Extension of the Helmholtz Integral Equation Method to Shorter Wavelengths," preprint.
[7]See, for example, J. C. Balomey and A. Wirgin, "Numerical Comparison of the Green's Function and the Waterman and Rayleigh Theories of Scattering from a Cylinder with Arbitrary Cross Section," Proc. IEEE 121, 794–804 (1974), and references therein.
[8]P. C. Waterman, "Matrix Theory of Elastic Wave Scattering," J. Acoust. Soc. Am. 60, 567–579 (1976).
[9]Y.-H. Pao and V. Varatharajulu, "Huygen's Principle, Radiation Conditions, and Integral Formulas for the Scattering of Elastic Waves," J. Acoust. Soc. Am. 59, 1361–1371 (1976); V. Varatharajulu and Y.-H. Pao, "Scattering Matrix for Elastic Waves. I. Theory," J. Acoust. Soc. Am. 60, 556–566 (1976).
[10]A. Boström, "Scattering of Stationary Acoustic Waves by an Elastic Immersed in a Fluid," J. Acoust. Soc. Am. 67, 390–398 (1980).
[11]L. Lewin, "On the Restricted Validity of Point Matching Techniques," IEEE Trans. Microwave Theory Tech. MTT-18, 1041–1047 (1970).
[12]R. H. T. Bates and D. J. N. Wall, "Null Field Approach to Scalar Diffraction I. General Method," Philos. Trans. R. Soc. Lond. Ser. A 287, 45–78 (1977).
[13]D. J. N. Wall, Ph.D. thesis, University of Canterbury, England (1976).
[14]D. J. N. Wall, "Circularly Symmetric Green Tensors for the Harmonic Wave Equation in Spheroidal Coordinate Systems," J. Phys. A: Gen. 11, 749–757 (1978).
[15]D. J. N. Wall, "The Null Field Approach to the Antenna Boundary Value Problem," IEEE International Conf. on Antennas and Propagation. Part I, 174 (1979).
[16]D. J. N. Wall, "Methods of Overcoming Numerical Instabilities Associated with the *T*-Matrix Method," in *Acoustic, Electromagnetic and Elastic Wave Scattering*, edited by V. V. Varadan and V. K. Varadan (Pergamon, New York, 1980), pp. 269–286.
[17]W. M. Visscher, "Method of Optimal Truncation: A New *T*-Matrix Approach to Elastic Wave Scattering," in *Acoustic, Electromagnetic and Elastic Wave Scattering*, edited by V. V. Varadan and V. K. Varadan (Pergamon, New York, 1980), pp. 287–301.
[18]M. F. Werby and L. H. Green, "An Extended Unitary Approach for Acoustical Scattering from Elastic Shells Immersed in a Fluid," J. Acoust. Soc. Am. 74, 625–630 (1983).
[19]A. Boström, "Scattering of Acoustic Waves by a Layered Elastic Obstacle in a Fluid—An Improved Null Field Approach," J. Acoust. Soc. Am. 76, 588–593 (1984).
[20]A. Lakhtakia, V. K. Varadan, and V. V. Varadan, "Iterative Extended Boundary Condition Method for Scattering by Objects of High Aspect Ratios," J. Acoust. Soc. Am. 76, 906–912 (1984).
[21]P. C. Waterman, "Surface Fields in Potential Theory and Acoustic Scattering," J. Acoust. Soc. Am. 76, 1215–1226 (1984).
[22]P. C. Waterman, "Survey of *T*-Matrix Methods and Surface Field Representations," in *Acoustic, Electromagnetic and Elastic Wave Scattering*, edited by V. V. Varadan and V. K. Varadan (Pergamon, New York, 1980), pp. 61–78.
[23]P. C. Waterman, "Matrix Theory of Elastic Wave Scattering. II. A New Conservation Law," J. Acoust. Soc. Am. 63, 1320–1325 (1978).
[24]Y. H. Pao, "Betti's Identity and the Transition Matrix for Elastic Waves," J. Acoust. Soc. Am. 64, 302–310 (1978).
[25]R. H. Hackman, "The Transition Matrix for Acoustic and Elastic Wave Scattering in Prolate Spheroidal Coordinates," J. Acoust. Soc. Am. 75, 34–45 (1984).
[26]See, for example, C. Flammer, *Spheroidal Wave Functions* (Stanford U.P., Stanford, CA, 1957) in this regard.
[27]M. Kotani, Proc. Phys.-Math. Soc. Jpn. 15, 30 (1933).
[28]C. J. Bowkamp, "Theoretische en Numerieke Behandeling van de Buiging Door Een Vonde Opening," Diss. Groningen, Groningen-Batavia, 1941; also J. Math. Phys. 26, 79 (1947).
[29]R. D. Spence, "The Diffraction of Sound by Circular Disks and Apertures," J. Acoust. Soc. Am. 20, 380–386 (1948).
[30]R. D. Spence and S. Granger, "The Scattering of Sound from a Prolate Spheroid," J. Acoust. Soc. Am. 23, 701–706 (1951).
[31]T. B. A. Senior, "The Scattering from Acoustically Hard and Soft Prolate Spheroids for Axial Incidence," Can. J. Phys. 44, 655–667 (1966).
[32]A. A. Klëshchev and L. S. Sheiba, "Scattering of a Sound Wave by Ideal Prolate Spheroids," Sov. Phys. Acoust. 16, 219–222 (1970).
[33]A. A. Klëshchev, "Sound Scattering by Ideal Spheroids in the High Frequency Limit," Sov. Phys. Acoust. 19, 447–449 (1974).
[34]N. D. Kazarinoff and R. K. Ritt, "On the Theory of Diffraction and Its Application to the Prolate Spheroid," Ann. Phys. 6, 227–299 (1959).
[35]R. F. Goodrich and N. D. Kazarinoff, "Scalar Diffraction by Prolate Spheroids Whose Eccentricities Are Almost One," Proc. Cambridge Philos. Soc. 59, 167–183 (1963).
[36]B. D. Sleeman, "Integral Representations Associated with High Frequency Non-Symmetric Scattering by Prolate Spheroids," Q. J. Mech. Appl. Math. 22, 405–426 (1969); B. D. Sleeman, "On Diffraction at Short Wavelengths by a Prolate Spheroid," J. Inst. Math. Its Appl. 5, 432–442 (1969).
[37]G. C. Lauchle, "Short-Wavelength Acoustic Diffraction by Prolate Spheroids," J. Acoust. Soc. Am. 58, 568–575 (1975); G. C. Lauchle, "Short-Wavelength Acoustic Backscattering by a Prolate Spheroid," J. Acoust. Soc. Am. 58, 576–580 (1975).
[38]A. Silbiger, "Scattering of Sound by an Elastic Prolate Spheroid," J. Acoust. Soc. Am. 35, 564–570 (1963).
[39]C. Yeh, "Scattering of Acoustic Waves by a Penetrable Prolate Spheroid. I. Liquid Prolate Spheroids," J. Acoust. Soc. Am. 42, 518–521 (1967); C. Yeh, "The Diffraction of Sound Waves by Penetrable Disks," Ann. Physik 13, 53–61 (1964).
[40]F. L. DiMaggio and A. Silbiger, "Free Extensional Torsional Vibrations of a Prolate Spheroidal Shell," J. Acoust. Soc. Am. 33, 56–58 (1961); A. Silbiger and F. L. DiMaggio, "Extensional Axi-Symmetric Second Class Vibrations of a Prolate Spheroidal Shell," Contract No. Nonr 266(67), Tech. Rep. No. 3, Columbia University, 1961.
[41]N. Shiraishi and F. L. DiMaggio, "Perturbation Solution for the Axisymmetric Vibrations of Prolate Spheroidal Shells," J. Acoust. Soc. Am. 34, 1725–1731 (1962).
[42]P. J. Nemergut and R. S. Brand, "Axisymmetric Vibrations of Prolate Spheroidal Shells," J. Acoust. Soc. Am. 38, 262–265 (1965).
[43]F. DiMaggio and R. Rand, "Axisymmetric Vibrations of Prolate Spheroidal Shells," J. Acoust. Soc. Am. 40, 179–186 (1966).
[44]S. K. Datta and A. H. Shah, "Axially Symmetric Waves in an Elastic Solid of Revolution," J. Acoust. Soc. Am. 44, 473–47 (1968).
[45]R. H. Rand, "Torsional Vibrations of Elastic Prolate Spheroids," J. Acoust. Soc. Am. 44, 749–751 (1968).
[46]O. I. Grossman, A. A. Klëshchev, and I. I. Klyukin, "Scattering of an Axisymmetric Plane Sound Wave by a Spheroidal Elastic Shell," Trudy Leningrad, Korabelstr. Inst. 74, 31–36 (1970).
[47]T. L. Gutman and A. A. Klëshchev, "Diffraction of Elastic Waves by an Elastic Spheroid," Trudy Leningrad. Korablestroitel. Inst. (Trudy LOLKI) 91, 31–37 (1974).
[48]A. A. Klëshchev, "Debye Potentials for Three-Dimensional Vibrations of a Spheroid Elastic Shell," Sov. Phys. Acoust. 21, 293–294 (1975); A. A. Klëshchev, "Sound Scattering by an Oblate Spheroidal Elastic Shell," Sov. Phys. Acoust. 21, 571–573 (1976); A. A. Klëshchev, "Sound Scattering by a Spheroidal Body at an Interface," Sov. Phys. Acoust. 25, 78–79 (1979).
[49]C. T. Möglich, Ann. Phys. 83, 609 (1927).
[50]J. Meixner, Z. Naturforsch. 3A, 506 (1948).
[51]J. Meixner, Ann. Phys. 12, 227 (1953).
[52]C. Flammer, "Radiation from Electric and Magnetic Dipoles in the Presence of a Conducting Circular Disk," Tech. Rep. No. 49, Contract AF 19(604)–1296, Stanford Research Institute (1955).
[53]F. V. Schultz, "Studies in Radar Cross-Section I—Scattering by a Prolate Spheroid," University of Michigan Rep. UMM-42 (1950).
[54]L. M. Rauch, "Electromagnetic Scattering by an Oblate Spheroid," University of Michigan Rep. UMM-116 (1953).
[55]K. M. Siegel, B. H. Gere, I. Marx, and F. B. Sleator, "Studies in Radar Cross-Section XI—The Numerical Determination of the Radar Cross-Section of a Prolate Spheroid, University of Michigan Rep. UMM-126 (1953).
[56]K. M. Siegel, F. V. Schultz, B. H. Gere, and F. B. Sleator, "The Theoretical and Numerical Determination of the Radar Cross-Section of a Prolate Spheroid," IRE Trans. Antennas Propag. AP-4, 266–275 (1956).
[57]S. Asano and G. Yamamoto, "Light Scattering by a Spheroidal Particle," Appl. Opt. 14, 29–49 (1975).
[58]S. Asano, Appl. Opt. 18, 712 (1979).
[59]M. Kotlarchyk, S.-H. Chen, and S. Asano, "Accuracy of RGD Approximation for Computing Light Scattering Properties of Diffusing and Motile Bacteria," Appl. Opt. 18, 2470–2479 (1979).
[60]S. Asano and M. Sato, "Light Scattering by Randomly Oriented Spheroidal Particles," Appl. Opt. 19, 962–974 (1980).
[61]S. Asano, "Light Scattering by Horizontally Oriented Spheroidal Particles," Appl. Opt. 22, 1390–1396 (1983).
[62]A. L. Van Buren, R. V. Baier, and S. Hanish, "A FORTRAN Computer Program for Calculating the Oblate Spheroidal Radial Functions of the First and Second Kind and Their First Derivatives," NRL Report 6959

(Jan. 1970).
[63]B. J. King, R. V. Baier, and S. Hanish, "A FORTRAN Computer Program for Calculating the Prolate Spheroidal Radial Functions of the First and Second Kind and Their First Derivatives," NRL Report 7012 (March 1970).
[64]B. J. King and A. L. Van Buren, "A FORTRAN Computer Program for Calculating the Prolate and Oblate Angle Functions of the First Kind and Their First and Second Derivatives," NRL Report 7161 (Nov. 1970).
[65]See, for example, B. J. Patz and A. L. Van Buren, "A FORTRAN Computer Program for Calculating the Prolate Spheroidal Angular Functions of the First Kind," NRL Memorandum Report 4414 (March 1981).
[66]There are a number of measures of the condition of a matrix. To be specific in this paper we adopt Von Neumann and Goldstine's P-condition number

$$P(A)=\lambda_{\max}/\lambda_{\min},$$

as the standard for the measure of condition. Here, $\lambda_{\max}$ and $\lambda_{\min}$ are the largest and smallest eigenvalues of the matrix A in absolute magnitude. A good general reference is J. R. Westlake, *A Handbook of Numerical Matrix Inversion and Solution of Linear Equations* (Wiley, New York, 1968).
[67]See, for example, G. Strang, *Linear Algebra and Its Applications* (Academic, New York, 1976), pp. 96–145.
[68]The relevant literature is reviewed in J. D. Achenbach, *Wave Propagation in Elastic Solids* (North-Holland, New York, 1976), pp. 240–249.
[69]L. R. Dragonette, "Evaluation of the Relative Importance of Circumferential or Creeping Waves in the Acoustic Scattering from Rigid and Elastic Solid Cylinders and from Cylindrical Shells," NRL Report No. 8216 (1978).
[70]For example, see Richard K. Cook, "Acoustics," in *American Institute of Physics Handbook*, edited by D. E. Gravy (McGraw-Hill, New York, 1963), pp. 3-88. Cook gives a 10% variation in μ and no variation in λ.
[71]L. Flax, V. K. Varadan, and V. V. Varadan, "Scattering of an Obliquely Incident Acoustic Wave by an Infinite Cylinder," J. Acoust. Soc. Am. **68**, 1832–1835 (1980).
[72]J.-H. Su, V. V. Varadan, V. K. Varadan, and L. Flax, "Acoustic Wave Scattering by a Finite Elastic Cylinder in Water," J. Acoust. Soc. Am. **68**, 686–691 (1980).
[73]S. K. Numrich, V. V. Varadan, and V. K. Varadan, "Scattering of Acoustic Waves by a Finite Elastic Cylinder Immersed in Water," J. Acoust. Soc. Am. **70**, 1407–1411 (1981).
[74]P. M. Morse and H. Feshbach, *Methods of Theoretical Physics* (McGraw-Hill, New York, 1953), pp. 661.